Low-cost AlCl$_3$/Et$_3$NHCl electrolyte for high-performance aluminum-ion battery

Hanyan Xu, Tianwen Bai, Hao Chen, Fan Guo, Jiabin Xi, Tieqi Huang, Shengying Cai, Xingyuan Chu, Jun Ling[*], Weiwei Gao, Zhen Xu, Chao Gao[*]

MOE Key Laboratory of Macromolecular Synthesis and Functionalization, Department of Polymer Science and Engineering, Zhejiang University, 38 Zheda Road, Hangzhou 310027, PR China

A B S T R A C T

The aluminum-ion battery is a very promising rechargeable battery system for its high-power-density and three-electron-redox aluminum anode. Currently, the aluminum-ion battery is mainly composed of aluminum anode and graphitic cathode, separated by 1-ethyl-3-methylimidazolium chloride (EMIC)-based ionic liquid electrolyte. Despite of the progress made for cathode materials, its practical application is severely restricted by the high cost and low productivity of EMIC. Here we report a low-cost AlCl$_3$/Et$_3$NHCl room temperature ionic liquid electrolyte to fabricate practical yet high-performance Al-graphene battery. The battery shows 112 mAh g^{-1} cathodic capacity with 97.3% retention after 30,000 cycles and 84% retention even after an ultrahigh current density at 18 A g^{-1} (150 C, charged in 18 second). In this battery, electrochemical deposition/dissolution of aluminum at the anode while intercalation/de-intercalation of chloroaluminate anions in the graphene cathode take place during charge-discharge. The formation of a stage **3** graphene intercalation compound at fully charged state is confirmed. This pragmatic and cost-effective AlCl$_3$/Et$_3$NHCl room temperature ionic liquid grants the aluminum-ion battery with high performance and higher practical value.

1. Introduction

Explosive demand and consumption of clean and sustainable energy are in urgent need of novel secondary energy storage technologies based on earth-abundant, low-cost and environmental friendly components [1]. Lithium-ion batteries (LIBs) hardly meet these requirements due to the scarcity of lithium resources as well as high cost and potential safety concerns. Furthermore, its limited cycle life and poor power density have turned current researches toward other cost-effective energy storage systems with longer cycle life and higher rate capability [2–4]. With thousands of times higher power density than LIBs and long cycle life (> 100,000 cycles), carbon-based supercapacitors are promising devices but the lower energy density confines its further application [5,6]. In this regard, the novel Al-ion batteries (AIBs) have attracted much attention for its rich-reserved (8%), safety and high capacity aluminum metal anode (2978 mAh g^{-1} and 8034 mAh mL^{-1}) [2–4]. Remarkably, Dai and coworkers assembled an Al-graphite battery employing an ionic-liquid electrolyte mixed 1-ethyl-3-methylimidazolium chloride (EMIC) with anhydrous aluminum chloride (AlCl$_3$), achieving a breakthrough in performance (70 mAh g^{-1} specific capacity with

7500 cycles life) and opening up a new avenue for this high-power-density battery [3].

Subsequently, continuous efforts have been invested to achieve better performance by optimizing cathode materials [7–12], such as 3D graphite foam [9], graphene nanoribbons on highly porous 3D graphene foam [10], zeolite-templated carbon [11], and sulfur cathode [12]. Our group proposed and demonstrated a defect-free principal for designing cathode then as-designed graphene cathode exhibited high specific capacity, high-rate performance and superior cycling stability [13–16]. However, the above-mentioned researches depend enormously on the classical [EMIm]Al$_x$Cl$_y$ electrolyte, which severely restricts the grid-scale application and industrialization of AIBs due to the high cost and low productivity of EMIC. Consequently, developing a high-performance AIB using a cheap electrolyte is highly desired. A cheap AlCl$_3$/urea ionic liquid (IL) electrolyte was reported recently [17]. However, the resulting battery only displayed unsatisfactory performance (~500 cycles and 78 mAh g^{-1} at 0.1 A g^{-1}), and low preparation temperature was required (5 °C) to avoid the sublimation of AlCl$_3$ due to massive exotherm. Another low-cost AlCl$_3$/NaCl molten salt was proposed to assemble a battery with fine performance (190 mAh g^{-1} at 0.1 A g^{-1} yet 60 mAh g^{-1} at 4 A g^{-1}) [18], whereas

external heat (120 °C) was required to prepare and maintain the salt-based electrolyte. Therefore, it is still a great challenge to develop a low-cost and room temperature electrolyte enabling AIBs with high electrochemical performance.

Here we report a low-cost room temperature ionic liquid (RTIL) electrolyte mixed triethylamine hydrochloride (Et$_3$NHCl) with AlCl$_3$. The assembled AIB with Al-foil anode and graphene aerogel cathode shows high electrochemical performance: 112 mAh g^{-1} cathodic capacity with 97.3% retention after 30,000 cycles and 84% retention even after an ultrahigh current density at 18 A g^{-1} (150 C, charged in 18 second). These values are comparable with or better than those of [EMIm]Al$_x$Cl$_y$ electrolyte-based AIB. Significantly, the upper cut-off voltage of our battery is higher (~2.62 V) than that of [EMIm]Al$_x$Cl$_y$ case (2.45–2.54 V) thanks to the higher decomposition (oxidation) voltage of AlCl$_3$/Et$_3$NHCl, which was also demonstrated by density functional theory (DFT) calculations. In this Al-graphene (Al-G) battery, the metallic Al and dissolved AlCl$_4^-$ anions are transformed into Al$_2$Cl$_7^-$ anions on the anode side meanwhile AlCl$_4^-$ anions are extracted from the graphene layer during discharging. The reverse reaction takes place during charging. The low-cost AlCl$_3$/Et$_3$NHCl electrolyte sheds light on the application and industrialization of AIBs.

2. Experimental

2.1. Synthesis of graphene aerogel cathode

The cathode was prepared according to the previous work of our group [13]. Graphene oxide (GO) solution (4 mg ml^{-1}) was freeze-dried to obtain graphene aerogel (GA) which was then chemically reduced to get reduced graphene aerogel (rGA). The as-prepared rGA was annealed at high temperature to get defect-free GA cathode material. The characterization of rGA is shown in Fig. S1 (Supplementary material).

2.2. Synthesis of AlCl$_3$/Et$_3$NHCl ionic liquid

The electrolyte was made by mixing triethylamine hydrochloride (Et$_3$NHCl, 98.5%, TCI, previously heated in vacuum at 110 °C for 24 to remove residual water and oxygen) and certain (1.0–1.7) mole equivalent anhydrous aluminum chloride (AlCl$_3$, 98%, Sigma-Aldrich, use as bought) in glove box for 12 h to obtain transparent liquid in light yellow with conductivity 9.41 mS cm^{-1} at 303.15 K. This conductivity was tested by CON 80 benchtop conductivity meter (Trans-Wiggens).

2.3. Battery fabrication

Coin cell was fabricated with graphene aerogel cathode (0.3–0.8 mg cm^{-2}), aluminum(Al) foil anode, current collector of nickel foam for cathode, glass fiber paper (Whatman 934-AH, thickness of 435 µm) as separator and 160 µL electrolyte. Soft pack cell was fabricated with graphene aerogel cathode, Al foil anode, current collector of tantalum foil for cathode and glass fiber paper as separator and ~600 µL electrolyte. The aluminum symmetric cell was assembled by employing Al-foil as both working electrode and counter electrode, with glassy fiber as separator and AlCl$_3$/Et$_3$NHCl or [EMIm]Al$_x$Cl$_y$ as electrolyte. *In situ* Raman/XRD cells were constructed with cover glass to obtain optical access and sealed with tapes.

2.4. Electrochemical tests

Cyclic voltammogram (CV) was performed on a CHI600D Electrochemical Workshop (Shanghai, China) at a scan rate of 1~10 mV s^{-1} and voltage range of 0.7~2.54 V (or 2.60 V). The galvanostatic cycling was performed on a Land BT2000 Battery Test System (Wuhan, China) charged to 2.54 V (or 2.62 V) and discharged to 0.7 V at 5 A g^{-1}. Part of the rate performance tests were carried out on

Neware Battery Test System (Shenzhen, China) at different current densities. A three-electrode electrochemical measurements were used for testing CV of electrolyte. A glassy carbon electrode (diameter: 3 mm) was used as the working electrode, while aluminum spiral was used as the counter and reference electrodes, at a scan rate of 10 mV s^{-1}. The Coulombic efficiency of stripping/ deposition of Al in the electrolyte was tested at current density of 0.5 mA cm^{-2} on Land system. The testing cell was assembled using Al foil as counter electrode and tantalum foil as working electrode. The deposition capacity of Al was fixed at 0.01 mAh cm^{-2} at 0.5 mA cm^{-2} and the charging limiting voltage was set at 1 V to strip the Al [19].

2.5. Structural and chemical characterization

(*In situ*) Raman spectra were obtained from an inVia-Reflex micro-Raman spectroscopy system. The AlCl$_3$/Et$_3$NHCl samples were sealed in NMR tubes for Raman test. ^{27}Al NMR was recorded neat with a lock (sealed DMSO capillaries) and the reference was 1.0 M solutions of Al(NO$_3$)$_3$ in D$_2$O. The morphologies of the electrodes were investigated by scanning electron microscope (SEM) (Hitachi S-3000N). The elemental mapping results were obtained through an energy-dispersive spectrometer (EDS) linked to Hitachi S-3000N. X-ray photoelectron spectroscopy (XPS) analysis was collected on an Escalab250Xi spectrometer with an Mg (Kα) source. Powder *in-situ* X-ray diffraction (XRD) results were examined through a Bruker D8 X-ray diffractometer with Cu Kα1 radiation (1.5405 Å) in the scan range of 10–80°.

2.6. Calculation details

All geometries of intermediates were optimized using B3LYP/6–311++G(d,p) under tight criteria. Frequency calculation confirmed all intermediates have zero imaginary frequency. Thermal correction to Gibbs free energies was obtained at 298.2 K and 1.013 × 10^5 Pa. All calculations were performed using Gaussian 09 program as we reported before [20].

3. Results and discussion

The used Et$_3$NHCl salt is an intractable industrial waste, cheap and abundant [21]. We directly employed the commercial Et$_3$NHCl (98.5%) to prepare AlCl$_3$/Et$_3$NHCl electrolyte. The electrolyte was synthesized by mixing precisely Et$_3$NHCl with certain mole equivalent (mol equ.) AlCl$_3$ in glove box without external heating and transparent liquid in light yellow was then obtained (Fig. S2, Supplementary material). With increasing molar ratios (r$_{AlCl3}$), the fluidity of liquids became better gradually. Raman spectroscopy was then performed to investigate the speciation in AlCl$_3$/Et$_3$NHCl RTIL at different ratios (Fig. 1a). For the AlCl$_3$:Et$_3$NHCl=1.0 (r$_{AlCl3}$ = 1), only the peak at 347 cm^{-1} was detected, which is assigned to the Al-Cl terminal stretching frequencies in AlCl$_4^-$ anions. When the ratio was increased, two peaks at 309 and 429 cm^{-1} appeared, which are assigned to Al-Cl vibrations in Al$_2$Cl$_7^-$ anions [22–24]. With increasing ratios, the peak at 347 cm^{-1} was observed to become weak gradually yet the peak at 309 cm^{-1} strengthened. And this is attributed to the mentioned-below equilibria reactions in the chloroaluminate ILs. When AlCl$_3$ is dissolved into Et$_3$NHCl (r$_{AlCl3}$ < 1), tetracoordinate AlCl$_4^-$ is formed according to Eq. (1). As more than 1.0 mol equ. AlCl$_3$ (r$_{AlCl3}$ > 1) is added, AlCl$_4^-$ is transformed into oligomeric Al$_2$Cl$_7^-$ (even Al$_3$Cl$_{10}^-$), a Lewis *acidic*, according to Eqs. (2) and (3) [25]. Consequently, it was verified that AlCl$_3$/Et$_3$NHCl RTIL is consist of AlCl$_4^-$ and Al$_2$Cl$_7^-$ anions (r$_{AlCl3}$ > 1), which are indispensable anionic species for the reaction in Al-ion battery.
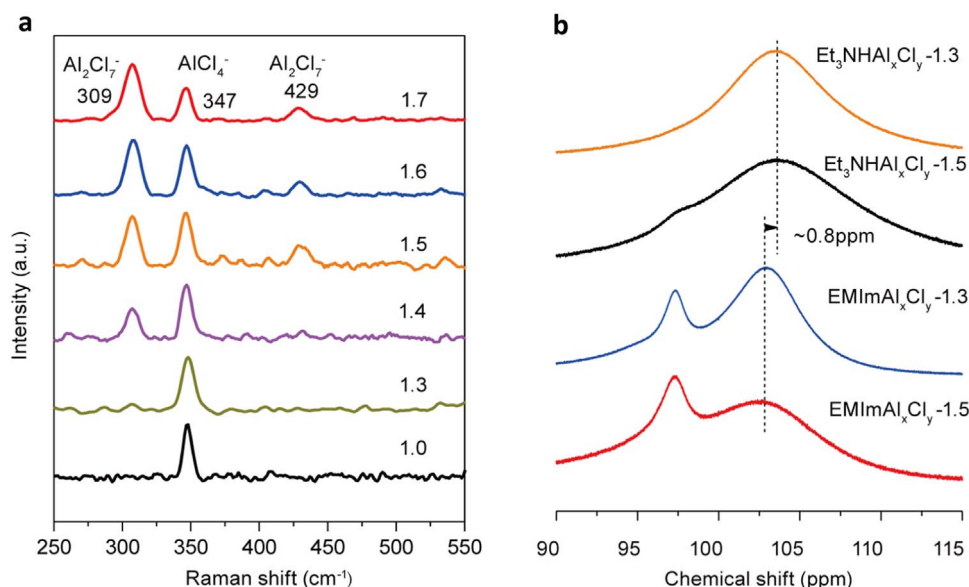
$$AlCl_3 + Cl^- \rightleftharpoons AlCl_4^- \tag{1}$$

$$2AlCl_4^- \rightleftharpoons Al_2Cl_7^- + Cl^- \tag{2}$$

$$AlCl_4^- + AlCl_3 \rightleftharpoons Al_2Cl_7^- \tag{3}$$

Fig. 1. a) Raman spectra of the AlCl₃/Et₃NHCl at different molar ratios. b) ^{27}Al NMR spectra of AlCl₃/Et₃NHCl and [EMIm]AlₓClᵧ at molar ratios of 1.3 and 1.5 (at ambient temperature). There is ~0.8 ppm difference of the indicated peaks.

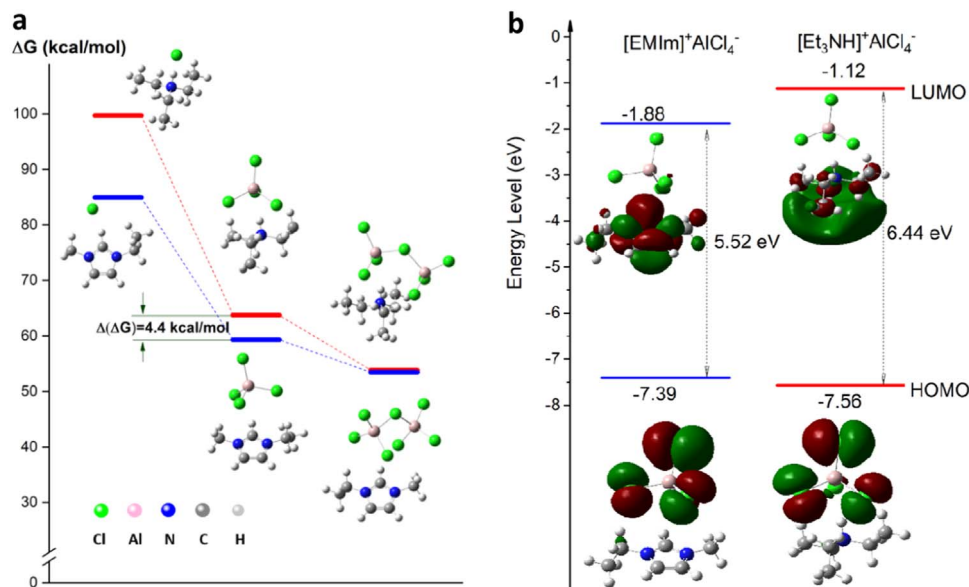**Fig. 2.** a) DFT calculated bonding energies of Et₃NH⁺ and [EMIm]⁺ with Cl⁻, AlCl₄⁻ and Al₂Cl₇⁻ with ΔG (kcal/mol) energies using B3LYP/6−311++G(d,p) method. b) HOMO and LUMO plots of [EMIm]⁺AlCl₄⁻ and [Et₃NH]⁺AlCl₄⁻ calculated by DFT.

Further, the influence of the cation on anions in AlCl₃/Et₃NHCl compared with [EMIm]AlₓClᵧ was analyzed by ^{27}Al NMR and DFT calculations. As shown in Fig. 1b, two resonances at 102.7 and 97.3 ppm are observed distinctly for [EMIm]AlₓClᵧ, but there are still partial overlaps. The two signals are assigned to AlCl₄⁻ and Al₂Cl₇⁻ anions, respectively [26]. By contrast, ^{27}Al NMR only featured one broadening peak (δ~103.5 ppm, AlCl₄⁻) for AlCl₃/Et₃NHCl at ratio 1.3, yet a weak resonance at 97.5 ppm (Al₂Cl₇⁻) appeared at 1.5. The overlapped signals of AlCl₄⁻ and Al₂Cl₇⁻ species are due to their fast dynamic equilibria (compared to NMR timescale) [25–28]. Especially, it would be more challenging to separate them when the tested chloroaluminate ILs with high viscosity. As a result, the main cause of weaker signal of Al₂Cl₇⁻ in AlCl₃/Et₃NHCl than in [EMIm]AlₓClᵧ derives from former higher viscosity, according to Table S1 [7,29]. Ionic interaction was then studied by DFT calculation to better understand the disparity between the two systems. According to the calculation results, [Et₃NH]⁺AlₓClᵧ⁻ pairs behave larger bonding energies in all cases

compared to [EMIm]⁺AlₓClᵧ⁻, as shown in the Fig. 2a. The bonding energy of [Et₃NH]⁺AlCl₄⁻ is 4.4 kcal/mol larger than that of [EMIm]⁺AlCl₄⁻. That means, on the one hand, the higher bonding energy leads to AlCl₃/Et₃NHCl with higher viscosity than EMIC-based case so that making difference in their NMR shifts, which is consistent with experimental and literature records; on the other hand, it can bring better stability to the AlCl₃/Et₃NHCl system.

Notably, the AlCl₄⁻ signal in AlCl₃/Et₃NHCl (103.5 ppm) moved to lower magnetic field than in [EMIm]AlₓClᵧ (102.7 ppm), which indicated the Al atom of AlCl₄⁻ anions in AlCl₃/Et₃NHCl receive more charge shielding from the cations. This difference would be reflected in the charge distribution and energy level in the two systems. Previous studies have demonstrated that the highest occupied molecular orbital (HOMO) is dominated by the anionic status while the lowest unoccupied molecular orbital (LUMO) is governed by the cationic status [30]. As shown in Fig. 2b, [Et₃NH]⁺AlCl₄⁻ pair exhibits lower HOMO and higher LUMO energy than that of [EMIm]⁺AlCl₄⁻, which in turn effects
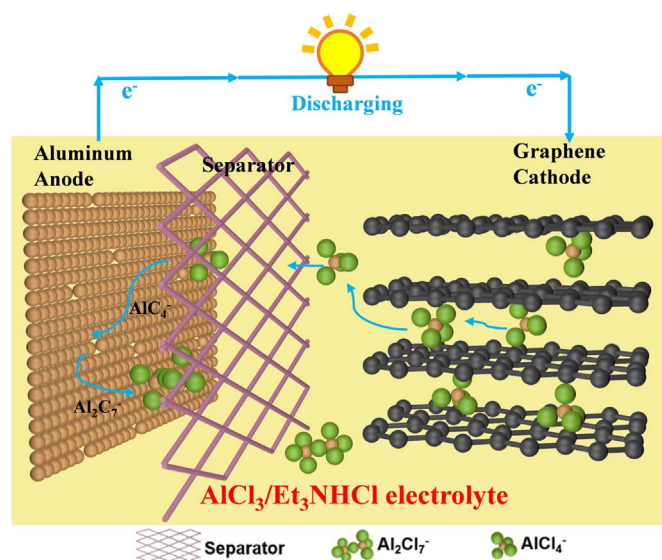
Fig. 3. Schematic of the Al-G battery based on the AlCl$_3$/Et$_3$NHCl electrolyte during discharging.

the anodic and cathodic limiting potential of the two ILs. Predictably, the AlCl$_3$/Et$_3$NHCl displays higher decomposition voltage and wider potential window than EMIC-based case.

Then the AlCl$_3$/Et$_3$NHCl RTIL was used as electrolyte in our AIB composed of Al-foil anode, graphene aerogel cathode and a separator as illustrated in Fig. 3. The optimization of molar ratio of AlCl$_3$/Et$_3$NHCl electrolyte is important for successful battery operation. Both considering the voltage and capacity of each battery consisting of electrolyte at different ratios (1.4–1.7), 1.5 was manifested as the best one (Fig. S3). So all following electrochemical performance of AIB was tested based on electrolyte at 1.5 if not mentioned.

Fig. 4a and Fig. S2 show the cyclic voltammogram (CV) curves of Al-G battery, and several oxidation peaks were observed in 1.8–2.2 V (V vs. Al/Al^{3+}) range while another well-defined peak appeared at 2.37 V (2.3–2.54 V). Corresponding reduction peaks emerged at 1.3–1.8 V and 2.2–1.94 V. The oxidation/reduction peaks and corresponding plateaus (Fig. 4b) confirmed the reversible cathodic intercalation/de-intercalation reaction illustrated in Fig. 3. In terms of anodic reaction, the CV curves of symmetric cell (Al-Al cell) exhibited reversible anodic peak at 0.5 V (dissolution of aluminum) and cathodic peak at −0.47 V (deposition of aluminum) at scan rate of 1 mV s^{-1} (Fig. 4c), demonstrating the stable and reversible aluminum plating/stripping reaction in AlCl$_3$/Et$_3$NHCl electrolyte. Compared with the conventional [EMIm]Al$_x$Cl$_y$ (r$_{AlCl3}$ = 1.3), the used AlCl$_3$/Et$_3$NHCl exhibited a faster plating/stripping reaction for its higher position of anodic/cathodic peaks and drastically increased peak current (Fig. 4c), which benefits to the efficiency of anodic reaction (95% for AlCl$_3$/Et$_3$NHCl while 91% for [EMIm]Al$_x$Cl$_y$, Fig. S3).

Fig. 4d shows the results of galvanostatic cycling test. The AlCl$_3$/Et$_3$NHCl electrolyte-based Al-G battery delivered 112 mAh g^{-1} cathodic capacity with average Coulombic efficiency over 98% and 97.3% retention after 30 000 cycles at a current density of 5 A g^{-1}. Rarely changed charge/discharge voltage plateaus were recognized with different cycles (Fig. 4e). As shown in Fig. 4f and Fig. S4, the high capacity over 100 mAh g^{-1} was well retained within wide current densities range from 0.5 to 12 A g^{-1} (4.2 C to 100 C, charged in 791 and 30 s, respectively) (Table S2). Impressively, the cathodic capacity remained at ~90 mAh g^{-1} (84% capacity retention) even at a high current density of 18 A g^{-1} (150 C, charged in 18 s), and the charge/discharge plateaus were still discerned despite the current density was raised to 20 A g^{-1} (167 C, charged in 15.3 s) (Fig. 4g). Overall, the excellent cycling stability and rate performance of our Al-G battery far

surpass previously reported Al-carbon batteries based on [EMIm]Al$_x$Cl$_y$ electrolyte (Fig. 4 h) [3,31], and low-cost electrolytes (Table S3) [17,18]. These advantages result from the good conductivity of AlCl$_3$/Et$_3$NHCl RTIL (9.41 ms cm^{-1}, 303.2 K) and the defect-free graphene cathode, facilitating the fast migration and intercalation of AlCl$_4^-$ [13,32–34]. Such an Al-G battery can afford an energy density of 56 Wh kg^{-1} comparable to lead–acid and Ni−MH batteries [35,36], and power density of 26 kW kg^{-1} comparable to supercapacitors (Fig. 4i) [37,38].

Given both discharging capacity and Coulombic efficiency, the charged cut-off voltage was determined at 2.54 (Fig. 4j, Fig. S6). Notably, our Al-G battery was able to operate under 2.62 V with specific capacity of 117 mAh g^{-1}, 6000 cycles life and average Coulombic efficiency over 96% (Fig. S7). By contrast, the Coulombic efficiency dropped significantly to 89% as the [EMIm]Al$_x$Cl$_y$ electrolyte-based Al-G battery was operated under 2.62 V. Previous studies have demonstrated that, for acidic chloroaluminate ILs, the cathodic limiting potential was associated with the electrodeposition of metallic Al while the anodic limiting potential was limited by chlorine evolution arising from the oxidation of anionic species [30,39,40]. Consequently, the higher upper voltage of our Al-G battery based on AlCl$_3$/Et$_3$NHCl electrolyte resulting from higher anodic voltage of AlCl$_3$/Et$_3$NHCl compared with [EMIm]Al$_x$Cl$_y$ (Fig. S8), which is consistent with the calculation of energy level as mentioned before.

To reveal the reaction mechanism at cathode, *in situ* Raman scattering was performed during a typical charging and discharging process (Fig. 5a). When charging to ~1.5 V, a slight splitting of the G-band of graphene (~1587 cm^{-1}) generated a blue upshift peak E$_{2g2}$(b) at 1609 cm^{-1} and an E$_{2g2}$(i) at ~1589 cm^{-1}, which was ascribed to the intercalation of AlCl$_4^-$ into graphene layer stacking [41,42]. The E$_{2g2}$(i) peak disappeared at ~2.3 V and E$_{2g2}$(b) finally converted into a new peak at 1638 cm^{-1} when fully charged at 2.54 V. The reversed shifts occurred during discharging. Therefore, *in situ* Raman spectroscopy confirmed powerfully the intercalation/de-intercalation of AlCl$_4^-$ anions in graphene cathode during charge-discharge [43,44]. X-ray photoelectron spectroscopy (XPS) showed C 1s peaks (sp^2 hybridized carbon ~284.5 eV), Al 2p peaks and Cl 2p peaks (Cl 2p$_{1/2}$~200.1 eV and Cl 2p$_{3/2}$~198.5 eV), demonstrating that the AlCl$_4^-$ anions were intercalated in graphene cathode (Fig. 5b, c, d) [3,45]. Element mapping also revealed that there were uniformly distributed Al and Cl elements in fully charged graphene cathode (Fig. 5e, f). Additionally, *in-situ* X-ray diffraction (XRD) spectra exhibited stage **3** graphene intercalation compound (GIC) at fully charged state, which is well matched with the value of cathodic capacity, calculated by the dominant peak (00n+1) at 22.2° and peak (00 n+2) at 27.9° based on Bragg's law (Fig. 5g) [32,46,47]. These tests verified that AlCl$_4^-$ anions were intercalated/de-intercalated into graphene layer during charge-discharge, and a stage **3** GIC with a [AlCl$_4^-$]/C ratio of 1/24 was obtained at fully charged state [48]. The chemical reaction on the electrodes during discharging can be described as following and illustrated at Fig. 3.

Anodic reaction: $Al + 7AlCl_4^- \rightarrow 4Al_2Cl_7^- + 3e^-$ (4)

Cathodic reaction: $C_{24}^+AlCl_4^- + e^- \rightarrow AlCl_4^- + C_{24}$ (5)

Postmortem scanning electron microscope (SEM) images of graphene cathode before/after 2000 cycles suggested that its graphene structure can tolerate the insertion and extraction of AlCl$_4^-$ anions with long cycles for its integrated framework (Fig. S9) [49,50]. On the other side, the morphology of Al anode verified that an ultrathin and continuous aluminum oxide as protective layer suppressed the growth of aluminum dendrite, ensuring the stable cycling of this Al-G battery based on AlCl$_3$/Et$_3$NHCl electrolyte (Fig. S10) [51].

4. Conclusions
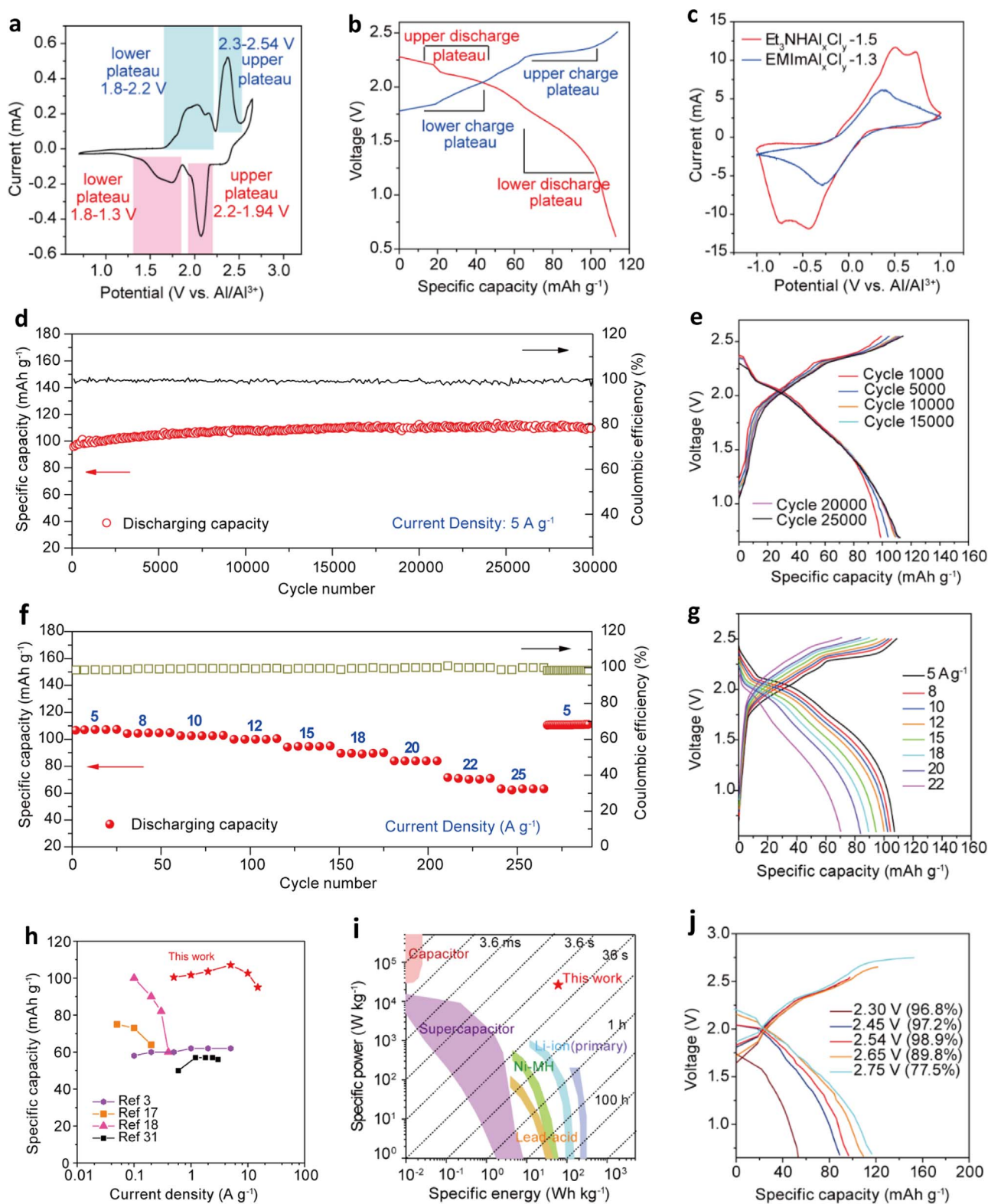
In summary, we report an AlCl$_3$/Et$_3$NHCl RTIL electrolyte with

Fig. 4. Electrochemical performance of the Al-G battery based on the AlCl$_3$/Et$_3$NHCl electrolyte at mole ratio of 1.5. a) Cyclic voltammogram (CV) curve at 1 mV s^{-1}. b) The representative galvanostatic charge/discharge curve at 5 A g^{-1}. c) CV curves of the symmetric cell consisting of AlCl$_3$/Et$_3$NHCl and [EMIm]Al$_x$Cl$_y$ (ratio 1.3) at 1 mV s^{-1}, respectively. d) Galvanostatic cycling over 3,000 cycles (current density at 5 A g^{-1} and 2.54 V/0.7 V upper/lower cut-off voltage). e) The typical galvanostatic curves at different cycles. f) Rate capability at different charge/discharge current densities from 5 A g^{-1} to 25 A g^{-1} and g) corresponding galvanostatic curves. h) Comparison of specific capacity and rate performance of this work with reported Al-carbon battery based on [EMIm]Al$_x$Cl$_y$ or cheap electrolyte. i) Comparison of energy/power density of our battery with the reported values of energy storage devices based on carbon electrode. j) Galvanostatic curves at different cut-off voltages (5 A g^{-1}) with Coulombic efficiency showed in brackets.
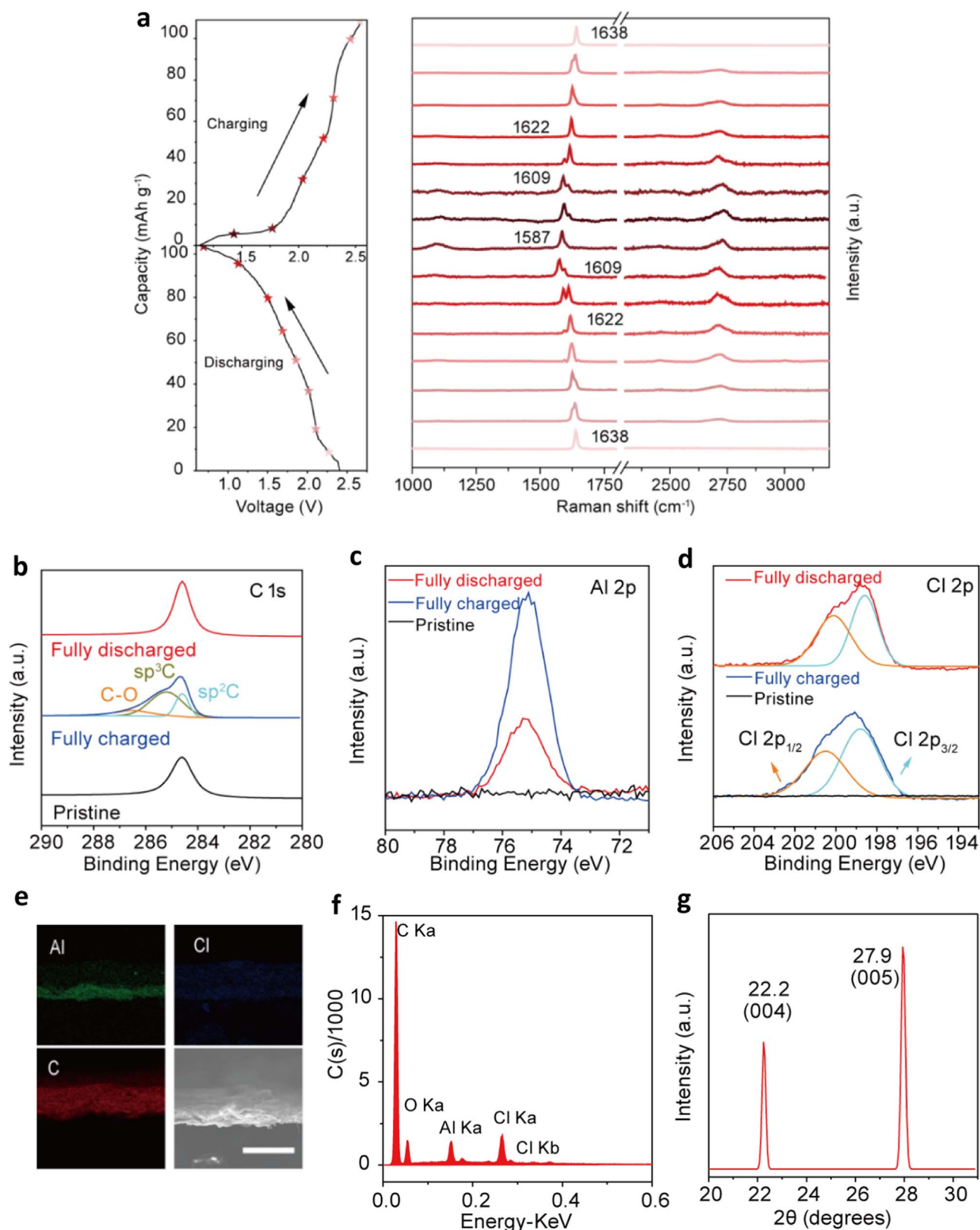
Fig. 5. The Al-G battery reaction mechanism at cathode. a) *In situ* Raman spectra of graphene cathode recorded during charging and discharging process. XPS peaks of b) C 1s, c) Al 2p and d) Cl 2p of the graphene cathode at pristine state and fully charged/discharged state. Peak-fit results are shown in different color lines. e) The images of SEM elemental mapping for C, Al and Cl elements, scar bar, 100 μm and f) the corresponding mapping spectrum. g) *In situ* XRD spectra of graphene cathode at fully charged state.

following four advantages:

(1) low-cost, commercial Et$_3$NHCl salt is 20–30x cheaper than EMIC while the industrial Et$_3$NHCl is even thousands of times cheaper (Table S4);
(2) added value, the intractable industrial waste (Et$_3$NHCl) is changed into a highly valuable electrolyte;
(3) high voltage, higher decomposition voltage leads to a wider potential window for AIB;
(4) long cycle, cycling stability and other high-performance make AIB highly promising.

The resulting Al-G battery displays cathodic capacity of 112 mAh g^{-1} with 97.3% retention after ultralong 30 000 cycles (42C) and retains high capacity over 100 mAh g^{-1} from 4.2C to 100C and ~90 mAh g^{-1} even at a ultrahigh rate 150 C. The performance is comparable with those of AIB with the classic expensive EMIC-based electrolyte overall. By various characterization strategies, the cathodic intercalation/de-intercalation and anodic deposition/dissolution mechanisms are revealed. We believe that such an electrolyte can be extended to AIB composed of other graphitic cathode materials. This low-cost AlCl$_3$/Et$_3$NHCl RTIL would pave the way for industrialization of Al-ion battery.

Declaration of interests

The authors declare no competing financial interest.

Acknowledgements

Appendix A. Supporting information

Supplementary data associated with this article can be found in the online version at doi:10.1016/j.ensm.2018.08.003.

References

[1] M. Armand, J.M. Tarascon, Building better batteries, Nature 451 (2008) 652.
[2] G.A. Elia, K. Marquardt, K. Hoeppner, S. Fantini, R. Lin, E. Knipping, W. Peters, J.F. Drillet, S. Passerini, R. Hahn, An overview and future perspectives of aluminum batteries, Adv. Mater. 28 (2016) 7564–7579.
[3] M.C. Lin, M. Gong, B. Lu, Y. Wu, D.Y. Wang, M. Guan, M. Angell, C. Chen, J. Yang, B.J. Hwang, H. Dai, An ultrafast rechargeable aluminium-ion battery, Nature 520 (2015) 324.
[4] S. Lee, J. Cho, Critical requirements for rapid charging of rechargeable al- and li-ion batteries, Angew. Chem. Int. Ed. 54 (2015) 9452–9455.
[5] L.L. Zhang, X.S. Zhao, Carbon-based materials as supercapacitor electrodes, Chem. Soc. Rev. 38 (2009) 2520–2531.
[6] H. Ji, X. Zhao, Z. Qiao, J. Jung, Y. Zhu, Y. Lu, L.L. Zhang, A.H. MacDonald, R.S. Ruoff, Capacitance of carbon-based electrical double-layer capacitors, Nat. Commun. 5 (2014) 3317.
[7] S. Xia, X.M. Zhang, K. Huang, Y.L. Chen, Y.T. Wu, Ionic liquid electrolytes for aluminium secondary battery: influence of organic solvents, J. Electroanal. Chem. 757 (2015) 167–175.
[8] Y. Hu, D. Ye, B. Luo, H. Hu, X. Zhu, S. Wang, L. Li, S. Peng, L. Wang, An innovative freeze-dried reduced graphene oxide supported SnS$_2$ cathode active material for aluminum-ion batteries, Adv. Mater. 29 (2017) 1606132.
[9] Y. Wu, M. Gong, M.C. Lin, C. Yuan, M. Angell, L. Huang, D.Y. Wang, X. Zhang, J. Yang, B.J. Hwang, 3D Graphitic foams derived from chloroaluminate anion intercalation for ultrafast aluminum-ion battery, Adv. Mater. 28 (2016) 9218–9222.
[10] X. Yu, B. Wang, D. Gong, Z. Xu, B. Lu, Graphene nanoribbons on highly porous 3D

[11] N.P. Stadie, S. Wang, K.V. Kravchyk, M.V. Kovalenko, Zeolite-templated carbon as an ordered microporous electrode for aluminum batteries, ACS Nano 11 (2017) 1911–1919.
[12] H. Yang, L. Yin, J. Liang, Z. Sun, Y. Wang, H. Li, K. He, L. Ma, Z. Peng, S. Qiu, C. Sun, H.M. Cheng, F. Li, An aluminum–sulfur battery with a fast kinetic response, Angew. Chem. Int. Ed. 130 (2018) 1916–1920.
[13] H. Chen, F. Guo, Y. Liu, T. Huang, B. Zheng, N. Ananth, Z. Xu, W. Gao, C. Gao, A defect-free principle for advanced graphene cathode of aluminum-ion battery, Adv. Mater. 29 (2017) 1605958.
[14] H. Chen, H. Xu, S. Wang, T. Huang, J. Xi, S. Cai, F. Guo, Z. Xu, W. Gao, C. Gao, Ultrafast all-climate aluminum-graphene battery with quarter-million cycle life, Sci. Adv. 3 (2017) eaao7233. http://dx.doi.org/10.1126/sciadv.aao7233.
[15] H. Chen, C. Chen, Y. Liu, X. Zhao, N. Ananth, B. Zheng, L. Peng, T. Huang, W. Gao, C. Gao, High-quality graphene microflower design for high-performance Li–S and Al-Ion batteries, Adv. Energy Mater. 7 (2017) 1700051.
[16] X. Zhao, W. Yao, W. Gao, H. Chen, C. Gao, Wet-Spun superelastic graphene aerogel millispheres with group effect, Adv. Mater. 29 (2017) 1701482.
[17] M. Angell, C.J. Pan, Y. Rong, C. Yuan, M.C. Lin, B.J. Hwang, H. Dai, High Coulombic efficiency aluminum-ion battery using an AlCl$_3$-urea ionic liquid analog electrolyte, Proc. Natl. Acad. Sci. USA 114 (2017) 834–839.
[18] S. Jiao, Y. Song, J. Tu, J. Wang, Y. Liu, H. Jiao, X. Mao, Z. Guo, D. Fray, A long-life rechargeable Al ion battery based on molten salts, J. Mater. Chem. A 5 (2017) 1282–1291.
[19] C.P. Yang, Y.X. Yin, S.F. Zhang, N.W. Li, Y.G. Guo, Accommodating lithium into 3D current collectors with a submicron skeleton towards long-life lithium metal anodes, Nat. Commun. 6 (2015) 8058.
[20] M. Frisch, G. Trucks, H. B. Schlegel, G. Scuseria, M. Robb, J. Cheeseman, G. Scalmani, V. Barone, B. Mennucci, G. Petersson, Gaussian 09, revision a. 02, gaussian, Inc., Wallingford, CT 200 (2009).
[21] A. Helin, T. Rönkkö, J. Parshintsev, K. Hartonen, B. Schilling, T. Läubli, M.L. Riekkola, Solid phase microextraction Arrow for the sampling of volatile amines in wastewater and atmosphere, J. Chromatogr. A 1426 (2015) 56–63.
[22] F. Coleman, G. Srinivasan, M. Swadźba-Kwaśny, Lewis supercidic ionic liquids with tricoordinate borenium cations, Angew. Chem. Int. Ed. 54 (2015) 14970–14973.
[23] S. Takahashi, L. Curtiss, D. Gosztola, N. Koura, M.-L. Saboungi, Molecular orbital calculations and Raman measurements for 1-ethyl-3-methylimidazolium chloroaluminates, Inorg. Chem. 34 (1995) 2990–2993.
[24] R. Gale, B. Gilbert, R. Osteryoung, Raman spectra of molten aluminum chloride: 1-butylpyridinium chloride systems at ambient temperatures, Inorg. Chem. 17 (1978) 2728–2729.
[25] J. Estager, J. Holbrey, M. Swadźba-Kwaśny, Halometallate ionic liquids–revisited, Chem. Soc. Rev. 43 (2014) 847–886.
[26] J.L. Gray, G.E. Maciel, Aluminum-27 nuclear magnetic resonance study of the room-temperature melt aluminum trichloride butylpyridinium chloride, J. Am. Chem. Soc. 103 (1981) 7147–7151.
[27] C. Ferrara, V. Dall'Asta, V. Berbenni, E. Quartarone, P. Mustarelli, Physicochemical characterization of AlCl$_3$–1-ethyl-3-methylimidazolium chloride ionic liquid electrolytes for aluminum rechargeable batteries, J. Phys. Chem. C 121 (2017) 26607–26614.
[28] J.W. Akitt, W. Gessner, M. Weinberger, High-field aluminium-27 nuclear magnetic resonance investigations of sodium aluminate solutions, Magn. Reson. Chem. 26 (2010) 1047–1050.
[29] A.A. Fannin Jr, D.A. Floreani, L.A. King, J.S. Landers, B.J. Piersma, D.J. Stech, R.L. Vaughn, J.S. Wilkes, J.L. Williams, Properties of 1, 3-dialkylimidazolium chloride-aluminum chloride ionic liquids. 2. phase transitions, densities, electrical conductivities, and viscosities, J. Phys. Chem. 88 (1984) 2614–2621.
[30] H. Wang, S. Gu, Y. Bai, S. Chen, N. Zhu, C. Wu, F. Wu, Anion-effects on electrochemical properties of ionic liquid electrolytes for rechargeable aluminum batteries, J. Mater. Chem. A 3 (2015) 22677–22686.
[31] G. Yang, L. Chen, P. Jiang, Z. Guo, W. Wang, Z. Liu, Fabrication of tunable 3D graphene mesh network with enhanced electrical and thermal properties for high-rate aluminum-ion battery application, RSC Adv. 6 (2016) 47655–47660.
[32] S.C. Jung, Y.J. Kang, D.J. Yoo, J.W. Choi, Y.K. Han, Flexible few-layered graphene for the ultrafast rechargeable aluminum-ion battery, J. Phys. Chem. C 120 (2016) 13384–13389.
[33] Y. Liu, Z. Xu, J. Zhan, P. Li, C. Gao, Superb electrically conductive graphene fibers via doping strategy, Adv. Mater. 28 (2016) 7941–7947.
[34] L. Kou, Y. Liu, C. Zhang, L. Shao, Z. Tian, Z. Deng, C. Gao, A Mini, Review on nanocarbon-based 1D macroscopic fibers: assembly strategies and mechanical properties, Nano-Micro Lett. 9 (2017) 51.
[35] I. Hadjipaschalis, A. Poullikkas, V. Efthimiou, Overview of current and future energy storage technologies for electric power applications, Renew. Sust. Energ. Rev. 13 (2009) 1513–1522.
[36] M. Winter, R.J. Brodd, What are batteries, fuel cells, and supercapacitors?, Chem. Rev. (35) (2004) 4245.
[37] T. Lin, I.W. Chen, F. Liu, C. Yang, H. Bi, F. Xu, F. Huang, Nitrogen-doped mesoporous carbon of extraordinary capacitance for electrochemical energy storage, Science 350 (2015) 1508–1513.
[38] X. Yang, C. Cheng, Y. Wang, L. Qiu, D. Li, Liquid-mediated dense integration of graphene materials for compact capacitive energy storage, Science 341 (2013) 534–537.
[39] S.I. Hsiu, J.F. Huang, I.W. Sun, C.H. Yuan, J. Shiea, Lewis acidity dependency of the electrochemical window of zinc chloride–1-ethyl-3-methylimidazolium chloride

ionic liquids, Electrochim. Acta 47 (2002) 4367–4372.

[40] T. Jiang, M.C. Brym, G. Dubé, A. Lasia, G. Brisard, Electrodeposition of aluminium from ionic liquids: part I—electrodeposition and surface morphology of aluminium from aluminium chloride (AlCl₃)–1-ethyl-3-methylimidazolium chloride ([EMIm] Cl) ionic liquids, Surf. Coat. Technol. 201 (2006) 1–9.

[41] A.S. Childress, P. Parajuli, J. Zhu, R. Podila, A.M. Rao, A Raman spectroscopic study of graphene cathodes in high-performance aluminum ion batteries, Nano Energy 39 (2017) 69–76.

[42] M. Balabajew, H. Reinhardt, N. Bock, M. Duchardt, S. Kachel, N. Hampp, B. Roling, In-situ Raman study of the intercalation of bis(trifluoromethylsulfonyl) imid ions into graphite inside a dual-ion cell, Electrochim. Acta 211 (2016) 679–688.

[43] L.J. Hardwick, M. Hahn, P. Ruch, M. Holzapfel, W. Scheifele, H. Buqa, F. Krumeich, P. Novák, R. Kötz, An in situ Raman study of the intercalation of supercapacitor-type electrolyte into microcrystalline graphite, Electrochim. Acta 52 (2006) 675–680.

[44] D. Zhan, L. Sun, Z.H. Ni, L. Liu, X.F. Fan, Y. Wang, T. Yu, Y.M. Lam, W. Huang, Z.X. Shen, FeCl₃-based few-layer graphene intercalation compounds: single linear dispersion electronic band structure and strong charge transfer doping, Adv. Funct. Mater. 20 (2010) 3504–3509.

[45] S. Yu, W. O'grady, D. Ramaker, P. Natishan, Chloride ingress into aluminum prior to pitting corrosion an investigation by XANES and XPS, J. Electrochem. Soc. 147 (2000) 2952–2958.

[46] G. Schmuelling, T. Placke, R. Kloepsch, O. Fromm, H.-W. Meyer, S. Passerini, M. Winter, X-ray diffraction studies of the electrochemical intercalation of bis (trifluoromethanesulfonyl) imide anions into graphite forádual-ion cells, J. Power Sources 239 (2013) 563–571.

[47] H. Kim, J. Hong, G. Yoon, H. Kim, K.-Y. Park, M.-S. Park, W.-S. Yoon, K. Kang, Sodium intercalation chemistry in graphite, Energy Environ. Sci. 8 (2015) 2963–2969.

[48] Y. Gao, C. Zhu, Z. Chen, G. Lu, Understanding ultrafast rechargeable aluminum-ion battery from first-principles, J. Phys. Chem. C 121 (2017) 7131–7138.

[49] L. Zhang, L. Chen, H. Luo, X. Zhou, Z. Liu, Large-sized few-layer graphene enables an ultrafast and long-life aluminum-ion battery, Adv. Energy Mater. 7 (2017) (1700034).

[50] Y. Liu, Z. Xu, W. Gao, Z. Cheng, C. Gao, Graphene and other 2D colloids: liquid crystals and macroscopic fibers, Adv. Mater. 29 (2017) 1606794.

[51] H. Chen, H. Xu, B. Zheng, S. Wang, T. Huang, F. Guo, W. Gao, C. Gao, Oxide film efficiently suppresses dendrite growth in aluminum-ion battery, Acs. Appl. Mater. Interfaces 9 (2017) 22628–22634.